RAA 2021 Vol. **21** No. **8**, 194(5pp) doi:10.1088/1674-4527/21/8/194

http://www.raa-journal.org *http://iopscience.iop.org/raa*

Research in Astronomy and Astrophysics

Quantifying the anisotropic density structure of the Central Molecular Zone – a 2D correlation function approach

Xiu-Yu Cai (蔡秀玉)[1,2], Guang-Xing Li (李广兴)[3] and Lei Qian (钱磊)[1]

[1] National Astronomical Observatories, Chinese Academy of Sciences, Beijing 100101, China; *lqian@nao.cas.cn*
[2] University of Chinese Academy of Sciences, Beijing 100049, China
[3] South-Western Institute for Astronomy Research, Yunnan University, Kunming 650500, China; *gxli@ynu.edu.cn*

Received 2020 December 24; accepted 2021 March 23

Abstract The Central Molecular Zone (CMZ) is a ring-like structure sitting at the center of the Milky Way. Using the 870 μm continuum map from the APEX Telescope Large Area Survey of the Galaxy (ATLASGAL), we study anisotropy in the density structure of gas in the CMZ utilizing the 2D correlation function. To quantify the spatial anisotropy, we define the critical angle $\theta_{\rm half}$, as well as the anisotropy parameter $A \equiv \frac{\pi}{4\theta_{\rm half}} - 1$. We find that the density structure is strongly anisotropic at a large scale ($\sim$ 100 pc), and the degree of spatial anisotropy decreases with decreasing scale. At the scale of $\sim$ 10 pc, the structure is still mildly anisotropic. In our analyses, we provide a quantitative description of the anisotropic density structure of gas in the CMZ, and the formalism can be applied to different regions to study their differences.

Key words: galaxies: ISM — ISM: molecules — ISM: structure

1 INTRODUCTION

Situated at the center of the Milky Way, the Central Molecular Zone (CMZ) is an unusually dense molecular cloud complex with a size of a few hundred parsecs (Launhardt et al. 2002). A total mass of $3 \times 10^7\,M_\odot$ is found inside this region (Dahmen et al. 1998; Molinari et al. 2014). Observations indicate that the gas in the CMZ has high volume densities (with a mean value of $\sim 10^4$ cm^{-3}, Li & Zhang 2020) and high column densities (about $\sim 10^{23}$ cm^{-2}, Lis & Carlstrom 1994).

In spite of the widespread presence of dense gas, the star formation efficiency (SFE) is about $10 - 100$ times lower than the standard values (Kauffmann et al. 2013; Longmore et al. 2013; Emsellem et al. 2015; Jeffreson et al. 2018). The dynamics in this region can be affected by a variety of processes, such as gravitational instability, turbulence, tidal force, cloud-cloud collision, shear, etc. (Longmore et al. 2013; Jeffreson et al. 2018; Kruijssen et al. 2019).

The shear on a cloud will cause a velocity difference between its near side and its far side with respect to the Galactic center, which stretches the gas into long streams. The strength of shear can be quantified using the shear timescale, which is $t_{\rm shear} = (\partial\Omega/\partial r \times r)^{-1}$. In the Milky Way, shear is believed to be responsible for creating large-scale filamentary structures (Dobbs & Bonnell 2006). Some first hints on the importance of shear came from the discovery of kpc-sized filamentary structures (Li et al. 2013; Goodman et al. 2014; Wang et al. 2015). Further observations have found that the filamentary structures with sizes of a few to a few tens of pc tend to stay parallel to the Galactic disk (Li et al. 2016; Wang et al. 2015), indicating that shear is dynamically important on these scales. In some cases, shear can play a dominant role in determining the star formation activity: recent results from Li & Zhang (2020) indicate that shear alone is responsible for the observed low level of star formation seen in the CMZ region.

One way to reveal the role of shear is to study the alignment of filamentary structures (Li et al. 2016; Wang et al. 2015). However, this approach, although effective, is cumbersome to implement. Besides, the evolution of the interstellar medium is a multi-scale process, and ideally, we would like to know the role of shear over a range of scales. As studying the role of shear considering the alignment of filamentary structures only allows us to probe the scales comparable to the lengths of the filaments, better methods are needed. In this paper, we develop a formalism to quantify the anisotropy of the density structure of the

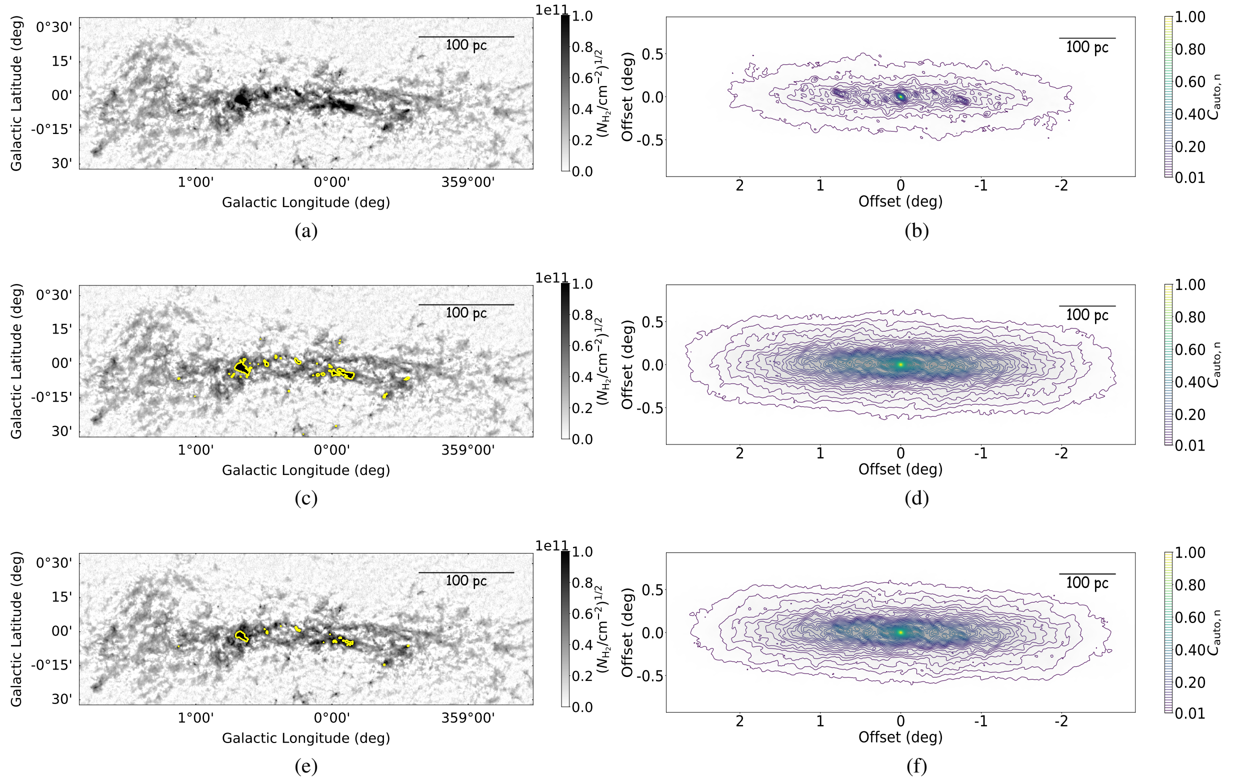

Fig. 1 *Left panels:* Column density distribution in the CMZ of the Galactic center observed by the survey: the ATLASGAL at 870 µm, with a beam size of 19.2″ and a typical noise level of 50–70 mJy beam^{-1}. The horizontal bar in the upper right corner indicates a length of 100 pc. The yellow contours in Fig. 1(c) indicate the region where the flux intensity is more than 3 Jy beam^{-1} (8.31×10^{21} cm^{-2}). The yellow contours in Fig. 1(e) signify the region where the flux intensity is more than 5 Jy beam^{-1} (1.385×10^{22} cm^{-2}). *Right panels:* 2D correlation functions $C_{\rm auto,n}$. In Fig. 1(b), the correlation function is computed using the emission map. In Figs. 1(d) and 1(f), we plot the correlation function computed from clipped emission maps where we set the value of regions where $I > 3$, 5 Jy beam^{-1} to $I_{\rm max}$ = 3, 5 Jy beam^{-1}, which correspond to $N_{\rm H_2} = 8.31 \times 10^{21}$ cm^{-2} and 1.385×10^{22} cm^{-2} respectively.

CMZ quantitatively applying the two-dimensional (2D) correlation function, with which the role of shear can be studied over a range of scales. In Section 2, we present the data. In Section 3, we describe the methods and present the results. In Section 4, we give a conclusion.

2 DATA

We examine the 870 µm map from the APEX Telescope Large Area Survey of the Galaxy (ATLASGAL) (Schuller et al. 2009). The observations were carried out with the APEX 12 m submillimeter telescope in dust emission continuum with an angular resolution of 19.2″ and a sensitivity of 50 mJy beam^{-1}. We assume that the CMZ region has a mean distance of 8.2 kpc, estimated from the updated distance to Sgr A from Gravity Collaboration et al. (2019). The corresponding spatial resolution is $\sim$ 0.76 pc. The size of the selected region is about 477 pc $\times$ 159 pc. The maps contain contaminations from the fore/background, and this amounts to around 10% of the total flux (Li & Zhang 2020). Thus, the contributions from fore/background emission to the overall correlation should be insignificant.

3 METHODS AND RESULTS

3.1 The Correlation Function

Our data are taken from Schuller et al. (2009), from which the column density can be calculated by utilizing

$$N_{\rm H_2} = \frac{F_\nu R_0}{B_\nu(T_{\rm D})\Omega\kappa\mu m_{\rm H}}, \tag{1}$$

where F_ν is the flux density, $R_0 \sim 100$ is the gas-to-dust ratio, Ω is the solid angle of the telescope beam, $\mu \sim 2.8$ is the mean molecular weight of the interstellar medium with respect to hydrogen molecules (Kauffmann et al. 2008) and $m_{\rm H}$ is the mass of a hydrogen atom. We adopt a uniform temperature of $T_{\rm D} = 20$ K (Ginsburg et al. 2016; Molinari et al. 2010; Traficante et al. 2011). At 870 µm, $\kappa = 1.85$ cm^2 g^{-1} (Ossenkopf & Henning 1994) and

$$B_\nu(T_{\rm D}) = \frac{2h\nu^3}{c^2}\frac{1}{e^{\frac{h\nu}{kT_{\rm D}}} - 1}\,. \tag{2}$$

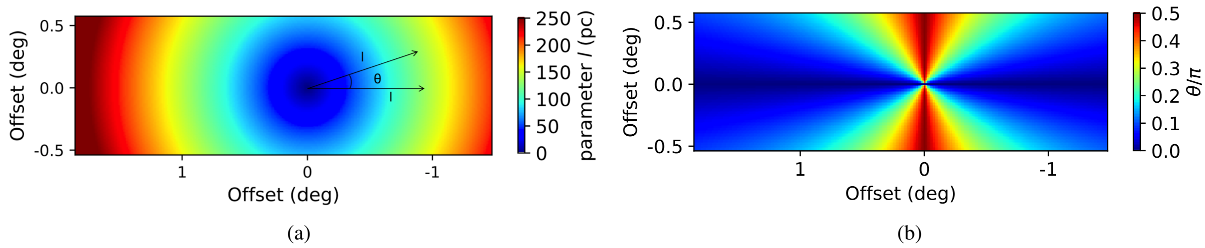

Fig. 2 (a) The region is divided with different radii and l is the distance from the origin. (b) The region is divided with different angles. We symmetrize it into the range of 0 to $\frac{\pi}{2}$. The colorbar is θ/π.

Here, we have assumed a uniform temperature for the whole region. In reality, the temperature varies by around 5 K, leading to an uncertainty of about 20% for individual regions. As the errors in column density caused by temperature variations are small compared to the intensity variations, the contribution from temperature to the overall correlation should be minimal.

To quantify the anisotropy of the density structure, we evaluate $C_{\rm auto}$, which is the 2D correlation function. Assuming that $f(x, y)$ represents the intensity distribution in the x–y plane, its Fourier transform is

$$f(k_1, k_2) = \int_{-\infty}^{\infty} \int_{-\infty}^{\infty} f(x, y) e^{-i(k_1 x + k_2 y)}\, dx dy. \quad (3)$$

We first calculate the power spectrum in k-space. $f^\dagger$ is the conjugate of f.

$$P(k_1, k_2) = f(k_1, k_2) f^\dagger(k_1, k_2). \quad (4)$$

Then the correlation function in the real space $C_{\rm auto}$ is obtained by the inverse transform

$$C_{\rm auto}(x, y) = \frac{1}{4\pi^2} \int_a^b \int_a^b P(k_1, k_2) e^{i(k_1 x + k_2 y)}\, dk_1 dk_2. \quad (5)$$

The column density map of the CMZ is displayed in Figure 1(a). The normalized 2D correlation function ($C_{\rm auto,n} \equiv C_{\rm auto}/C_{\rm auto,max}$) based on the flux data is shown in Figure 1(b). Note that calculations done in Fourier space assume a periodic boundary condition. To minimize boundary effects, we add zero paddings around our maps before performing the calculations. We note that in some cases, a very significant amount of emission is contained in a very small region (e.g. the Sgr B2 region). To evaluate their contributions to the overall correlation, we experiment with performing clipping operations to the data at regions where the flux is larger than a certain threshold of 3 Jy beam^{-1} (8.31×10^{21} cm^{-2}) and 5 Jy beam^{-1} (1.385×10^{22} cm^{-2}), separately. This is achieved by setting the values of regions where the flux is above a threshold to that threshold. We set flux data more than 3, 5 Jy beam^{-1} (8.31×10^{21} cm^{-2}, 1.385×10^{22} cm^{-2}) to $I_{\rm max}$ = 3, 5 Jy beam^{-1} (8.31×10^{21} cm^{-2}, 1.385×10^{22} cm^{-2}). The regions where the flux data are more than 3, 5 Jy beam^{-1} (8.31×10^{21} cm^{-2}, 1.385×10^{22} cm^{-2}) are marked yellow in Figure 1(c) and Figure 1(e), respectively. The clipping operation effectively reduces the dynamic range of the maps. The correlation functions computed from these clipped maps are presented in Figure 1(d) and Figure 1(f). By comparing the clipped results (Fig. 1(d) and Fig. 1(f)) to the unclipped ones (Fig. 1(b)), we are able to evaluate the contribution to the correlation function from regions with different column densities.

From all these correlation functions, we observe that the contours in the center (at small scales) are nearly roundish, but at larger scales, the contours are elliptical where the long axes of the ellipses are aligned with the mid-plane of the Milky Way. This is an indication that shear is dynamically important in the region.

3.2 Quantifying the Spatial Anisotropy

To further quantify the spatial anisotropy measured as a function of the scale, we divide the region into rings of different radii. Each ring is characterized by the l parameter, which is the distance from the origin (Fig. 2(a)). For each ring, we plot the value of the correlation function against θ, which is the angle measured with respect to the Galactic mid-plane. We have considered all the points. In addition, θ has been transformed to the range $(0, \frac{\pi}{2})$ (Fig. 2(b)). Due to symmetry, θ is between 0 and π. Additionally, we assume that the structure of the CMZ is symmetric had we turned it upside down (horizontal mirror symmetry). Thus, we only need to plot θ between 0 and $\frac{\pi}{2}$.

As an example, we plot the results from a ring at $l \sim 33.4 - 35.8$ pc. The ring width Δl is 10 pixels, about 2.4 pc. In Figure 3(a), we plot the $C_{\rm auto,n}$ against θ. Here, the spatial anisotropy can be seen from the fact that the correlation is stronger along the l direction where $\theta = 0$, but becomes weaker as θ increases.

To quantify the spatial anisotropy at scale l, we define the so-called half correlation angle $\theta_{\rm half}$,

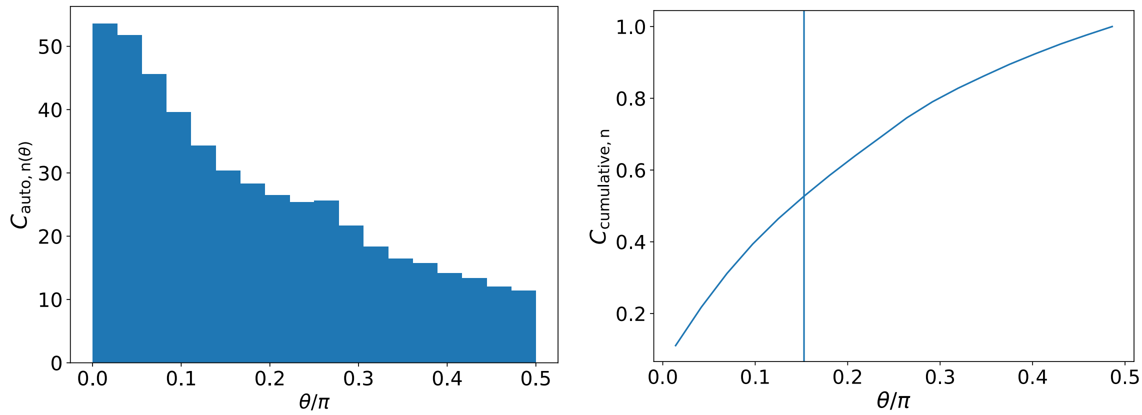

(a) (b)

Fig. 3 (a) The distribution of $C_{\mathrm{auto,n}}$ against θ. (b) $C_{\mathrm{cumulative,n}}$ - θ/π relation. $C_{\mathrm{cumulative,n}}$ is the normalized cumulative correlation function. The vertical line marks where $C_{\mathrm{cumulative,n}}$ is 0.5.

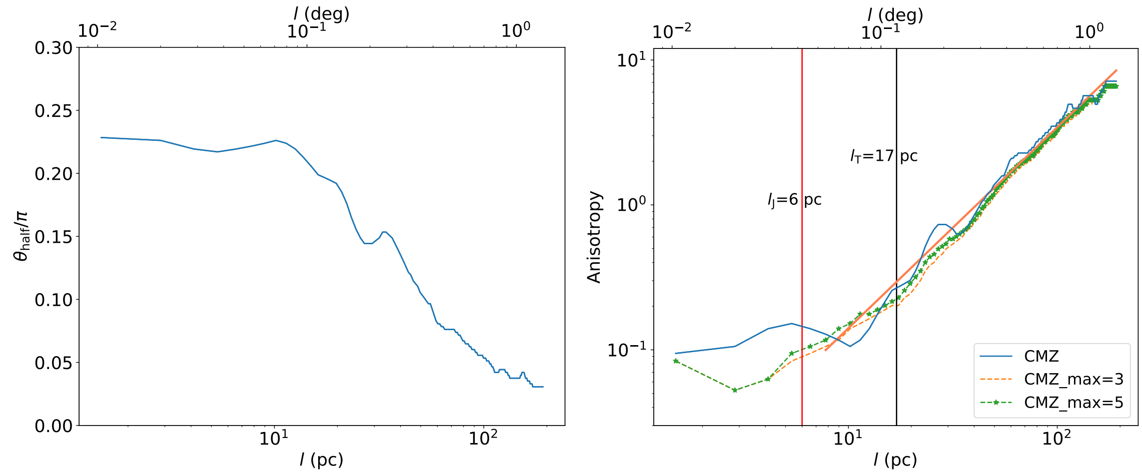

(a) (b)

Fig. 4 (a) $\theta_{\mathrm{half}}/\pi$ - l relation. θ_{half} decreases with l in the CMZ. (b) Anisotropy-l relation. The left vertical line indicates where the Jeans lengths l_{J} (6 pc) and the right vertical line represents the Toomre lengths l_{T} (17 pc) estimated by Henshaw et al. (2016). The solid line is the anisotropy-l distribution calculated with raw data. The dashed line is the anisotropy-l distribution calculated by setting raw data more than 3 Jy beam^{-1} (8.31×10^{21} cm^{-2}) to I_{max} = 3 Jy beam^{-1} (8.31×10^{21} cm^{-2}). The dashed line with stars is the anisotropy-l distribution calculated by setting raw data more than 5 Jy beam^{-1} (1.385×10^{22} cm^{-2}) to I_{max} = 5 Jy beam^{-1} (1.385×10^{22} cm^{-2}). The straight line at scales larger than 10 pc is the linear fit of data, $\log_{10} A \approx 1.4 \log_{10} l - 2.2$.

which is the critical angle within which half of the correlation function is contained. To derive θ_{half}, we define the so-called cumulative correlation function $C_{\mathrm{cumulative}}(\theta) = \int C_{\mathrm{auto,n}}(\theta)\mathrm{d}\theta$, then we normalize it, obtaining the normalized cumulative correlation function $C_{\mathrm{cumulative,n}}(\theta) = C_{\mathrm{cumulative}}(\theta)/C_{\mathrm{cumulative,max}}(\theta)$. θ_{half} is obtained by solving $C_{\mathrm{cumulative,n}}(\theta) = 0.5$. The procedure is illustrated in Figure 3(b). For isotropic structures, $\theta_{\mathrm{half}} = \frac{\pi}{4}$, whereas for structures that are preferentially aligned with the disk mid-plane, $\theta_{\mathrm{half}} < \frac{\pi}{4}$. An example of how we derive θ_{half} is presented in Figure 3(b).

The above-mentioned exercise allows us to study how the spatial anisotropy evolves as a function of the scale. In Figure 4(a), we plot θ_{half} against the scale, and where θ_{half} decreases with the increasing scale. This indicates that the spatial anisotropy is stronger at larger scales.

We further define the anisotropy parameter

$$A \equiv \frac{\pi}{4\,\theta_{\mathrm{half}}} - 1\,. \tag{6}$$

$A > 0$ means that at the scale of interest, the density structure is anisotropic, and the value of A measures the degree of anisotropy. For a homogeneous region, the correlation strength is evenly distributed between 0 and $\frac{\pi}{2}$. At $\theta_{\rm half} = \frac{\pi}{4}$, A will be 0. As $\theta = 0$ corresponds to the direction along which the correlation is concentrated, in most cases, $\theta_{\rm half} < \frac{\pi}{4}$ and $A > 0$. In Figure 4(b), we plot A against the scale. We also plot regions where we have chosen different $I_{\rm max}$. We note that at scales below 10 pc, the anisotropy parameter depends on the value of $I_{\rm max}$. Thus, we should only interpret results from scales larger than 10 pc, as only in this range do results from different $I_{\rm max}$ converge. At scales larger than 10 pc, we perform a fit to our data and find $\log_{10} A \approx 1.4 \log_{10} l - 2.2$. The anisotropy is strong on a large scale, and it decreases with decreasing scale. At around $l = 10$ pc, the density structure is still moderately anisotropic.

We further add the two vertical lines indicating the Toomre length $l_{\rm T} \approx 17$ pc and the Jeans length $l_{\rm J} \approx 6$ pc (Henshaw et al. 2016), respectively. The Jeans length is the length scale above which gravity can induce collapse, and the Toomre length is the length below which self-gravity is stronger than shear. The density structure is expected to be anisotropic at $l > l_{\rm T}$, and this is confirmed by our results. Apart from this, we can still observe a significant amount of anisotropy at $l_{\rm T} > l > l_{\rm J}$.

4 CONCLUSIONS

We study the density structure of gas in the CMZ by applying the 2D correlation function. We find that the density structure is strongly anisotropic where the correlation is strong along the l direction, suggesting that shear is dynamically important.

To quantify anisotropic density structure, we define the half-correlation angle $\theta_{\rm half}$ and the anisotropy parameter $A \equiv \frac{\pi}{4\theta_{\rm half}} - 1$. The density structure is strongly anisotropic at $l = 100$ pc, and is slightly anisotropic at $l = 10$ pc. Between 10 pc and 100 pc, we find that

$$\log_{10} A \approx 1.4 \log_{10} l - 2.2.$$

We propose a picture where at a large scale ($l > 10$ pc), shear is dynamically important such that it can change the density structure of the gas significantly, and its strength diminishes as one moves to smaller scales. At $l \lesssim 10$ pc, as shear should have roughly the same strength as self-gravity, the gas can enter a state called "shear-enabled pressure equilibrium" (Li & Zhang 2020). The formalism developed here can be applied to study the role of shear in different regions in a quantitative fashion and reveal the differences.

Acknowledgements We thank the anonymous referee for a constructive review report that improved this paper. Lei Qian is supported by the National Natural Science Foundation of China (NSFC, No. U1631237) and the Youth Innovation Promotion Association of CAS (id. 2018075). Guang-Xing Li is supported by a starting grant from Yunnan University, and NSFC (Nos. W820301904 and 12033005). The paper makes use of data from the ATLASGAL survey carried out by the APEX telescope.

References

Dahmen, G., Huttemeister, S., Wilson, T. L., & Mauersberger, R. 1998, A&A, 331, 959
Dobbs, C. L., & Bonnell, I. A. 2006, MNRAS, 367, 873
Emsellem, E., Renaud, F., Bournaud, F., et al. 2015, MNRAS, 446, 2468
Ginsburg, A., Henkel, C., Ao, Y., et al. 2016, A&A, 586, A50
Goodman, A. A., Alves, J., Beaumont, C. N., et al. 2014, ApJ, 797, 53
Gravity Collaboration, Abuter, R., Amorim, A., et al. 2019, A&A, 625, L10
Henshaw, J. D., Longmore, S. N., & Kruijssen, J. M. D. 2016, MNRAS, 463, L122
Jeffreson, S. M. R., Kruijssen, J. M. D., Krumholz, M. R., & Longmore, S. N. 2018, MNRAS, 478, 3380
Kauffmann, J., Bertoldi, F., Bourke, T. L., Evans, N. J., I., & Lee, C. W. 2008, A&A, 487, 993
Kauffmann, J., Pillai, T., & Zhang, Q. 2013, ApJL, 765, L35
Kruijssen, J. M. D., Dale, J. E., Longmore, S. N., et al. 2019, MNRAS, 484, 5734
Launhardt, R., Zylka, R., & Mezger, P. G. 2002, A&A, 384, 112
Li, G.-X., Urquhart, J. S., Leurini, S., et al. 2016, A&A, 591, A5
Li, G.-X., Wyrowski, F., Menten, K., & Belloche, A. 2013, A&A, 559, A34
Li, G.-X., & Zhang, C.-P. 2020, ApJ, 897, 89
Lis, D. C., & Carlstrom, J. E. 1994, ApJ, 424, 189
Longmore, S. N., Bally, J., Testi, L., et al. 2013, MNRAS, 429, 987
Molinari, S., Swinyard, B., Bally, J., et al. 2010, A&A, 518, L100
Molinari, S., Bally, J., Glover, S., et al. 2014, in Protostars and Planets VI, eds. H. Beuther, R. S. Klessen, C. P. Dullemond, & T. Henning, 125
Ossenkopf, V., & Henning, T. 1994, A&A, 291, 943
Schuller, F., Menten, K. M., Contreras, Y., et al. 2009, A&A, 504, 415
Traficante, A., Calzoletti, L., Veneziani, M., et al. 2011, MNRAS, 416, 2932
Wang, K., Testi, L., Ginsburg, A., et al. 2015, MNRAS, 450, 4043